Effects of Torsional Flexibility on An Unmanned Helicopter Performance Including Compressibility Effect

Alaaddin Furkan Uzunkaya, ASELSAN, Middle East Technical University, Ankara, Turkey
Prof. Dr. Yavuz Yaman, Middle East Technical University, Ankara, Turkey

Abstract

In this study, torsional deformation of an unmanned helicopter and its effect on the performance characteristics are examined. In the analyses, blade-element momentum theory is used for the calculation of the aerodynamic loads by implementing compressibility corrections. For the interactions between the aerodynamic loads and torsional deformations, an iterative solution procedure is developed. To obtain the trim points of the helicopter, a trim code is written in which blade is modeled as either rigid or elastic in the torsional direction. It is found that there occur some differences between the rigid and elastic blade in terms of the control inputs. However, since the aerodynamic center is close to the shear center of the reference blade, the difference is found to be negligible small. Therefore, effects of the torsional deformations on the helicopter control and performance are minimal.

1. NOTATION

Symbols

B	Tip loss factor
c	Chord of the blade, m
$c_d, c_{d_0}, c_{d_{\alpha^2}}$	Non-dimensional drag coefficient, zero-lift and second-order drag constants
c_l, c_{l_α}	Non-dimensional lift coefficient and lift-curve slope
D'	Drag force of blade element, N
e	Non-dimensional flap hinge offset
F_r, F_x, F_z	Radial, horizontal, and vertical force components of the blade, N
$H^{a,b}$	Harmonic solution constant
h	Vertical distance between rotor hub and center of gravity of the helicopter, m
$\widehat{I_a}, \widehat{I_b}$	Main rotor blade second-order and hinged second-order inertia, kg*m^2
i	Rotor incidence angle, rad
GJ	Torsional rigidity, N*m^2
L'	Lift force of blade element, N
M	Mach number
M'	Aerodynamic pitching moment of blade element span, N
M_H	Rotor hub moment, N*m
M_X, M_{XF}	Rotor hub and fuselage aerodynamic rolling moment, N*m
M_Y, M_{YF}	Rotor hub and fuselage aerodynamic pitching moment, N*m
M_{XX}, M_{YY}	Re-arranged rotor longitudinal and lateral hub moments, Nm
N_{az}, N_b, N_{bem}	Number of azimuth steps, blades of main rotor, blade elements
P	Compressibity factor
r	Radial distance between the blade element and rotor hub, m
r_R	Aerodynamic root cutout, m
T	Thrust of the main rotor,
U	Resultant air velocity, m/s
u_p, u_r, u_T	Perpendicular, radial, and tangential air velocity of the blade element, m/s
V	Forward flight speed of the helicopter, m/s
X_{CG}, Y_{CG}	Distance between CG of the helicopter and the rotor hub in x and y axes in body fixed frame respectively, m
X, Y	Horizontal and lateral force of the main rotor, N
X_F, Y_F	Aerodynamic drag and lateral force of the helicopter, N
x_{ac}, x_{ea}	Aerodynamic center and elastic axis location of the airfoil from the leading edge, m
α	Angle of attack, rad
$\beta, \beta_0, \beta_{1c}, \beta_{1s}$	Rotor flapping, coning, longitudinal, and lateral flap angles, rad
Δr	Length of the blade elements, m
η	Piecewise function to define vertical displacement of the blade, m

$\theta, \theta_0, \theta_{1c}, \theta_{1s}, \theta_{tw}$ Blade pitch, collective input, lateral, longitudinal, and elastic twist angle, rad
μ Non-dimensional forward speed
ν, ν_i Total and induced inflow, m/s
ξ Non-dimensional flap frequency
ρ Density of air, kg/m^3
Φ Rotor lateral tilt angle, rad
ϕ Inflow angle, rad

2. INTRODUCTION

Helicopters are the aircraft which rotates their blades to fly. Since the relative motion between the air medium and the blades are obtained by rotating the blades, helicopters are capable of vertical take-off and landing. Transporting, searching, and rescuing, could be given as examples of the areas where the helicopters are widely used.

In comprehensive helicopter analysis tools, helicopter blades could be modeled as rigid beams. However, it is well known that the helicopter blades are flexible structures. Main objective of this work to examine the effects of the torsional deformations of the main rotor blade on the helicopter's performance metrics and control inputs. In this study, aerodynamic loads are assumed to be steady, and the inflow of the main rotor is assumed to be uniform over the main rotor. To obtain aerodynamic load field of the main rotor, blade element momentum theory is implemented by including compressibility effect. Aerodynamic loads cause a torsional twist which alters the aerodynamic load field on the blade.

To be able to obtain the performance characteristics of the reference helicopter, a trim code is written which models the reference blade as either rigid or elastic.

An unmanned cargo helicopter and its main rotor blades are used as the reference helicopter in the study. In Table 1, reference helicopter design specifications and main rotor blade mechanical properties are given.

Table 1: Reference Helicopter and Main Rotor Blade Properties

Properties	Metric
MTOW	160 kg
Payload	40 kg
Length	2.07 m
Width	0.78 m
Height	1.22 m
CG w.r.t Rotor Hub in x-Body	~0 m
CG w.r.t Rotor Hub in y-Body	~0 m
CG w.r.t Rotor Hub in z-Body	0.4 m
Max Speed	125 km/h
Number of Blades	2

3. AERODYNAMIC LOADS

As mentioned before, blade element momentum theory is used to obtain the aerodynamic load field on the main rotor blades in which blades are divided into finite-length blade elements. Aerodynamic forces are calculated for these blade elements individually. Leishman (Ref. 1) stated that it is better to use at least 40 blade elements to preserve the aerodynamic load information. Therefore, reference main rotor blade is divided into 40 blade elements as could be seen in Figure 1.

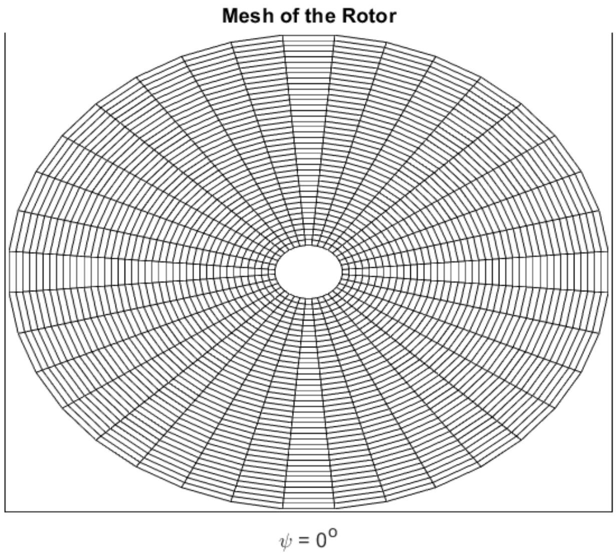

Figure 1: Reference Helicopter Main Rotor Mesh.

According to Johnson (Ref. 2), aerodynamic loads on the blade is very low up to 20% radius of the rotor due to the low dynamic pressure. This region is called as aerodynamic root cutout and denoted by r_R. In addition, due to the three-dimensional effects, blade does not produce any aerodynamic lift after approximately 97% of its radius (Ref. 1) which is called as tip loss effect and it is denoted by BR where B is called as tip loss factor. In this study, it is assumed that there is no aerodynamic force on the blade in the aerodynamic root cutout region and no aerodynamic lift force is produced after the 97% of reference blade's radius.

Aerodynamic forces of a blade element are given in (Ref. 3) as:

(1) $$L' = \frac{1}{2}\rho U^2 c c_l \Delta r$$

(2) $$D' = \frac{1}{2}\rho U^2 c c_d \Delta r$$

U in Eq's. (1) and (2) is the total airspeed experienced by the blade element and it could be approximated to the tangential velocity of the blade element as $U \cong \Omega r + V\, sin\psi$. According to (Ref. 4), lift and drag coefficient of the reference NACA 0012 blade has a linear and second order polynomial characteristic w.r.t to the angle of attack respectively such that $c_l = c_{l_\alpha}\alpha$ and $c_d = c_{d_0} + c_{d_{\alpha^2}}\alpha^2$. Lift curve slope, zero-lift drag coefficient and second order drag coefficient of the reference airfoil could be approximated as $c_{l_\alpha} = 5.93$, $c_{d_0} = 6.53x10^{-3}$ and $c_{d_{\alpha^2}} = 2.78x10^{-1}$. Angle of attack α is the difference between blade pitch angle and the ratio of vertical airspeed to the tangential velocity of the blade element $\alpha = \theta - \phi$ where the vertical velocity component of the blade element is:

(3) $$u_P = v + r\dot{\beta} + \beta V\, cos\,\psi$$

v is the inflow and assumed to be uniform over the main rotor and β is the flap angle of the blade which is going to be discussed in the following section.

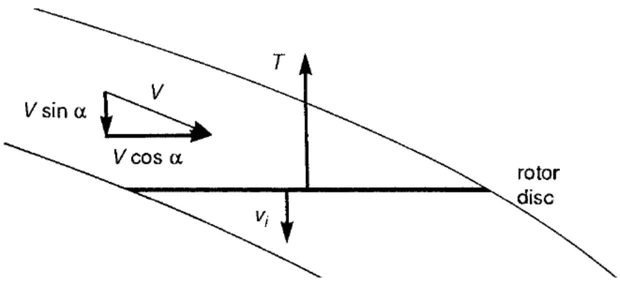

Figure 2: Inflow of the Main Rotor in Forward Flight (Ref. 4).

According to the Johnson (Ref. 2), total inflow of the main rotor v could be written as:

(4) $$v = \frac{v_i^2}{\sqrt{(V\,cos\,i)^2 + (V\,sin\,i + v)^2}}$$

where induced inflow is $v_i^2 = T/2\rho\pi R^2$. Thrust of the main rotor T could be approximated by summing the lift force of all blade elements between aerodynamic root cutout and tip loss.

(5) $$T \cong N_b \sum_{n=1}^{n=N_{bem}} (L')_n$$

If Eq's. (4) and (5) are inspected in detail, it is seen that thrust and inflow are coupled. Therefore, they could be solved by using an iterative solution procedure such that inflow is calculated by assuming that thrust of the main rotor is equal to the weight of the helicopter. Then aerodynamic lift forces of the blade elements are calculated for a given control input, i.e., blade pitch θ. By summing the lift force of the blade elements, new thrust could be obtained to obtain new inflow of the main rotor. After finding inflow, thrust is calculated and iteration procedure continues until convergence is obtained.

4. COMPRESSIBILITY CORRECTIONS

Ref. 1 states that airfoil characteristics are affected when experienced Mach number is greater than 0.3. In Figure 3, experienced local Mach number of the main rotor for hover and maximum forward flight speed is given. According to Figure 3, local Mach number of the reference blade could reach up to 0.65 in hover and 0.75 at the advancing side in maximum speed forward flight. Therefore, compressibility correction should be included in the aerodynamic loading calculations to increase fidelity. Anderson (Ref. 6) suggests that Prandtl-Glauert correction formula could be used to obtain lift-curve characteristics of the airfoil for a compressible condition if incompressible lift-curve slope is known. Prandtl-Glauert correction factor is given as:

(6) $$P = \frac{1}{\sqrt{1 - M^2}}$$

where P is the correction factor and M is the Mach number. By using Eq. (6), compressible lift-curve slope could be obtained by:

(7) $$c_{l_\alpha}^{comp} = \frac{c_{l_\alpha}^{incomp}}{\sqrt{1 - M^2}}$$

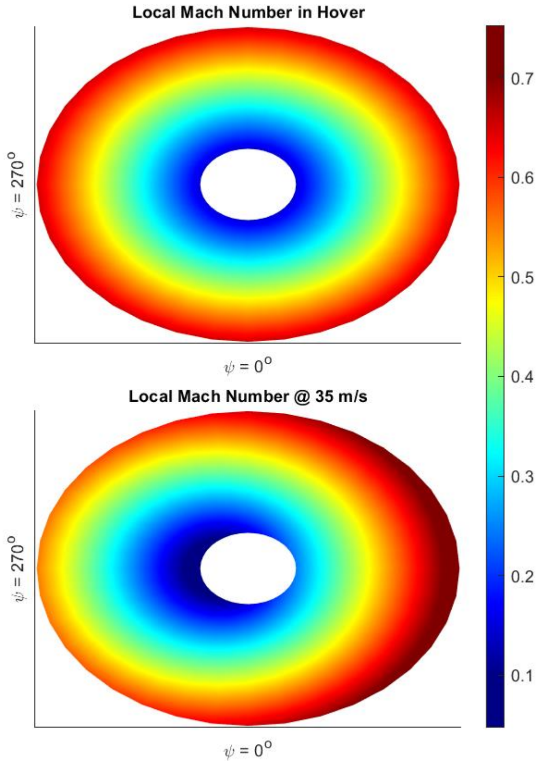

Figure 3: Local Mach Number in Hover and Forward Flight.

5. FLAPPING MOTION

Aerodynamic load field on the blade is azimuth varying in forward flight since the airspeed experienced by the blade changes with azimuth of the blade as could be seen from Figure 3. Due to this azimuth varying load field, blade makes an out-of-plane motion called as flapping. In (Ref. 3), flapping motion of the blade could be described as following:

(8) $$\beta = \beta_0 + \beta_{1s} \sin\psi + \beta_{1c} \cos\psi$$

However, Eq. (8) is valid for the blades which are connected to the rotor hub with a flap hinge. To be able to use Eq. (8), blades of a hingeless rotor are assumed to make the flap motion about an imaginary flap-hinge at a distance eR from the rotor hub where e is called as equivalent flap hinge offset. e is obtained by drawing a tangent line to the 75% radius of the blade's first out-of-plane bending mode shape as illustrated in Figure 4. Equivalent flap hinge offset is given in (Ref. 3) as:

(9) $$e_{eq} = \frac{\frac{2}{3}(\xi^2 - 1)}{1 + \frac{2}{3}(\xi^2 - 1)}$$

where ξ is the non-dimensional natural frequency ratio which is the first out-of-plane natural frequency to the rotor speed $\xi = \omega_h/\Omega$. For the reference blade ξ is 1.08, equivalent flap hinge offset e is 0.1.

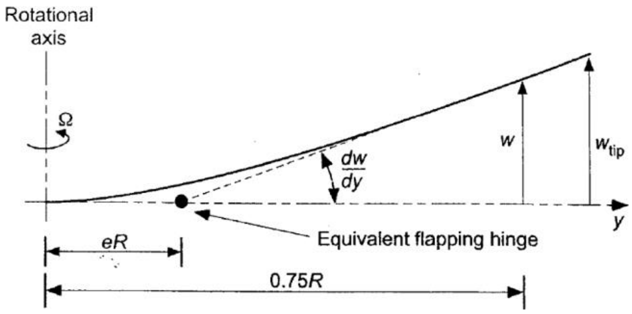

Figure 4: Equivalent Flapping Hinge Offset (Ref. 1).

Since the blade is flapping about the imaginary flap hinge, a piecewise function should be introduced to define the vertical displacement of the blade according to Johnson (Ref. 3):

(10) $$\eta = \begin{cases} \dfrac{r - eR}{1 - e} & r \geq eR \\ 0 & r < eR \end{cases}$$

After defining the vertical displacement of the blade w.r.t the flap hinge, flapping angle of the blade could be written as following by according to Ref. 7:

(11) $$\ddot{\beta} + (\xi\Omega)^2\beta \cong \frac{1}{\widehat{I_b}} \sum_{r_R}^{BR} L'\eta$$

where $\widehat{I_b}$ is the hinged second order inertia and $\widehat{I_b} = \int_{eR}^{R} \eta^2 m dr$ and also note that since flap hinge offset is less than the aerodynamic root cutout, summation limits in Eq. (11) are given from end of the root cutout to the tip loss. By using the vertical displacement definition given in Eq. (10), vertical velocity component u_p of the blade element could be re-written as $u_P = v + \eta\dot{\beta} + u_R\eta'\beta$.

6. ELASTIC TWIST

Blade pitch angle θ consists of two terms. First one is the control input, and it could be expressed as similar to the blade flapping in Eq. (8):

(12) $$\theta_{con} = \theta_0 + \theta_{1s} \sin\psi + \theta_{1c} \cos\psi$$

Second part of the blade pitch angle is the elastic torsional deformation of the blade, and it is denoted by θ_{tw}. Expression to find the torsional deformation of the blade is given in (Ref. 8) as following:

$$M' = GJ\frac{d\theta_{tw}}{dr} \tag{13}$$

where M' is the aerodynamic pitching moment. Since the airfoil symmetric it is assumed that aerodynamic pitching coefficient of the airfoil is zero; therefore, M' could be related to the blade element's aerodynamic lift force as following:

$$M' \cong L'(x_{ea} - x_{ac}) \tag{14}$$

By combining Eq's. (13) and (14), it is obtained:

$$GJ\frac{d\theta_{tw}}{dr} = \frac{1}{2}\rho c c_{l_\alpha} P u_T^2(\theta - \phi)(x_{ea} - x_{ac}) \tag{15}$$

Since tangential velocity u_T and compressibility factor P are also a function of radial distance, and there is blade elastic twist θ_{tw} term in the blade pitch angle θ, differential equation in Eq. (15) is very hard to solve. Therefore, an iterative solution method is implemented in this study such that in the first iteration, it is assumed that θ_{tw} as zero. Then sectional aerodynamic pitching moment is found by using Eq. (14) for the given blade control input. After finding the aerodynamic pitching moment, Eq. (13) could be solved to obtain torsional deformation. Iteration procedure continues until the elastic twist of the blade converges. Note that this iterative solution procedure is valid only for a specific loading condition where the blade is loaded by a single point load; however, there is an aerodynamic load field on the blade. To obtain torsional twist field of the blade, it is assumed that lift forces of blade elements and elastic twists could be superposed. Under these assumptions elastic twist field of the blade could be written as:

$$\theta_{tw} = \begin{cases} \dfrac{M'_1 r + M'_2 r + \cdots + M'_n r}{GJ} & r_1 \geq r \\ \dfrac{M'_1 r_1 + M'_2 r + \cdots + M'_n r}{GJ} & r_2 \geq r > r_1 \\ \dfrac{M'_1 r_1 + M'_2 r_2 + \cdots + M'_n r}{GJ} & r_n \geq r > r_{n-1} \end{cases} \tag{16}$$

where $M'_1, M'_2, \ldots, M'_n$ are the sectional aerodynamic pitching moments of the corresponding blade elements and $r_1, r_2, \ldots, r_n$ are the distance of the blade elements' distance from the root of the blade. By using Eq. (16), elastic twist field of the blade could be found.

7. HARMONIC SOLUTION

If the relation between blade flapping and aerodynamic lift of the blade elements in Eq. (11) is written explicitly, it is observed that there will be lots of harmonic terms i.e., $sin\,\psi$ and $cos\,\psi$ terms including higher-order harmonics such as $sin^2\,\psi$ and $cos^2\,\psi$. Therefore, Johnson (Ref. 3) suggests using the numerical operators given in Eq. (17) to obtain steady-state solutions.

$$\frac{1}{N_{az}}\sum_{n=1}^{n=N_{az}}(\ldots)$$

$$\frac{2}{N_{az}}\sum_{n=1}^{n=N_{az}}(\ldots)\,cos\,\psi_n \tag{17}$$

$$\frac{2}{N_{az}}\sum_{n=1}^{n=N_{az}}(\ldots)\,sin\,\psi_n$$

where N_{az} is the total number of discretization points of one revolution which is chosen as 36 in this study as shown in Figure 1, ψ_n is the angle of n^{th} azimuth step and is defined as $\psi_n = 2\pi\, n/N_{az}$. If the operands given in Eq. (17) are applied to the flapping terms in Eq. (11), steady-state blade flapping angles are obtained as:

$$\frac{1}{N_{az}}\sum_{n=1}^{n=N_{az}}\left(\ddot{\beta}_n + (\xi\Omega)^2\beta_n\right) = (\xi\Omega)^2\beta_0$$

$$\frac{2}{N_{az}}\sum_{n=1}^{n=N_{az}}(\ddot{\beta}_n + (\xi\Omega)^2\beta_n)\,cos\,\psi_n \cong \Omega^2(\xi^2 - 1)\beta_{1c} \tag{18}$$

$$\frac{2}{N_{az}}\sum_{n=1}^{n=N_{az}}(\ddot{\beta}_n + (\xi\Omega)^2\beta_n)\,sin\,\psi_n \cong \Omega^2(\xi^2 - 1)\beta_{1s}$$

To apply the operands to the aerodynamic flapping moment term, summation order should be changed. Since aerodynamic lift force is continuous over both radial and rotational direction, order of blade element and azimuth summations could be changed such that aerodynamic flapping moment is summed over the azimuth first then blade element summation is done. If the operands applied to the aerodynamic flapping moment term in Eq. (11) and it is equated to the flapping angles as suggested in (Ref. 7), it is obtained:

$$(19)\quad \begin{aligned}(\xi\Omega)^2\beta_0 &= \frac{1}{\widehat{I_b}}\sum_{r_R}^{BR}\frac{1}{2}\rho c c_{l_\alpha}\Bigg(\theta_0\{(\Omega r_m)^2 H_m^{0,0} \\ &+ 2\Omega r_m V H_m^{1,0} + V^2 H_m^{2,0}\} \\ &+ \theta_{1s}\{(\Omega r_m)^2 H_m^{1,0} + 2\Omega r_m V H_m^{2,0} + V^2 H_m^{3,0}\} \\ &+ \beta_{1c}\{\Omega^2 r_m \eta_m H_m^{1,0} \\ &- \Omega r_m V \eta'_m H_m^{0,2} + \Omega V \eta_m H_m^{2,0} - V^2 \eta'_m H_m^{1,2}\} \\ &- \nu\{\Omega r_m H_m^{0,0} + V H_m^{1,0}\} \\ &+ \frac{1}{N_{az}}\sum_{n=1}^{n=N_{az}} P_{m,n}\, u_{T\,m,n}^2 \theta_{tw_{m,n}}\Bigg)\eta_m \Delta r\end{aligned}$$

$$(20)\quad \begin{aligned}&\Omega^2(\xi^2-1)\beta_{1c} \\ &= \frac{2}{\widehat{I_b}}\sum_{r_R}^{BR}\frac{1}{2}\rho c c_{l_\alpha}\Bigg(\theta_{1c}\{(\Omega r_m)^2 H_m^{0,2} \\ &+ 2\Omega r_m V H_m^{1,2} + V^2 H_m^{2,2}\} \\ &- \beta_0\{\Omega r_m V \eta'_m H_m^{0,2} + V^2 \eta'_m H_m^{1,2}\} \\ &- \beta_{1s}\{\Omega^2 r_m \eta_m H_m^{0,2} + \Omega r_m V \eta'_m H_m^{1,2} \\ &+ \Omega V \eta_m H_m^{1,2} + V^2 \eta'_m H_m^{2,2}\} \\ &+ \frac{1}{N_{az}}\sum_{n=1}^{n=N_{az}} P_{m,n}\, u_{T\,m,n}^2 \theta_{tw_{m,n}} \cos\psi_n\Bigg)\eta_m \Delta r\end{aligned}$$

$$(21)\quad \begin{aligned}&\Omega^2(\xi^2-1)\beta_{1s} \\ &= \frac{2}{\widehat{I_b}}\sum_{r_R}^{BR}\frac{1}{2}\rho c c_{l_\alpha}\Bigg(\theta_0\{(\Omega r)^2 H_m^{1,0} + 2\Omega r V H_m^{2,0} \\ &+ V^2 H_m^{3,0}\} + \theta_{1s}\{(\Omega r)^2 H_m^{2,0} \\ &+ 2\Omega r V H_m^{3,0} + V^2 H_m^{4,0}\} \\ &+ \beta_{1c}\{\Omega^2 r \eta H_m^{2,0} - \Omega r V \eta' H_m^{1,2} + \Omega V \eta H_m^{3,0} \\ &- V^2 \eta' H_m^{2,2}\} - \nu\{\Omega r H_m^{1,0} + V H_m^{2,0}\} \\ &+ \frac{1}{N_{az}}\sum_{n=1}^{n=N_{az}} P_{m,n}\, u_{T\,m,n}^2 \theta_{tw_{m,n}} \sin\psi_n\Bigg)\eta_m \Delta r\end{aligned}$$

where $H^{a,b}$ is the harmonic parameter used to express non-zero higher-order harmonics of the flapping moment term and it is defined as:

$$(22)\quad H^{a,b} = \frac{1}{N_{az}}\sum_{n=1}^{n=N_{az}} P_n \sin^a(\psi_n)\cos^b(\psi_n)$$

8. TRIM PROCEDURE

Trim points are one of the important metrics since performance analyses are done w.r.t these trim points. Blade flapping angles, rotor incidence and roll angle for a leveled trim flight are given in (Ref. 3) and (Ref. 7) as following:

$$(23)\quad \beta_{1c} = \frac{\frac{D}{T} + \frac{H}{T} - \frac{X_{CG}}{h} - \frac{D}{W} + \frac{M_{YF}}{Wh} + \frac{M_{YY}}{Wh}}{1 + \frac{N_b \Omega^2(\xi^2-1)\widehat{I_a}}{Wh}}$$

$$(24)\quad \beta_{1s} = \frac{\frac{Y_F}{T} + \frac{Y}{T} + \frac{Y_{CG}}{h} - \frac{Y_F}{W} - \frac{M_{XF}}{Wh} - \frac{M_{XX}}{Wh}}{1 + \frac{N_b \Omega^2(\xi^2-1)\widehat{I_a}}{Wh}}$$

$$(25)\quad i = \frac{X_{CG}}{h} + \frac{D}{W} - \frac{M_{YF}}{Wh} - \frac{M_Y}{Wh}$$

$$(26)\quad \Phi = \frac{Y_{CG}}{h} - \frac{Y_F}{W} - \frac{M_{XF}}{Wh} - \frac{M_X}{Wh}$$

where $\widehat{I_a}$ is called as second order inertia of the main rotor blade and defined as $\widehat{I_a} = \int_{eR}^{R} m\eta r dr$. H and Y are rotor horizontal and lateral forces which could be given by:

$$(27)\quad H = \frac{N_b}{N_{az}}\sum_{m=1}^{N_{bem}}\left(\sum_{n=1}^{n=N_{az}}\left(F_{x_{m,n}}\sin\psi_n + F_{r_{m,n}}\cos\psi_n\right)\Delta r\right)$$

$$(28)\quad Y = \frac{N_b}{N_{az}}\sum_{m=1}^{N_{bem}}\left(\sum_{n=1}^{n=N_{az}}\left(-F_{x_{m,n}}\cos\psi_n + F_{r_{m,n}}\sin\psi_n\right)\Delta r\right)$$

where F_x and F_r are horizontal and radial components of the blade element and they are defined as $F_x \cong L'\phi + D'$ and $F_r \cong -\beta F_z$ (Ref. 2). M_{XX} and M_{YY} are re-arranged rotor lateral and longitudinal moments. They are re-arranged to obtain $\left(1+\frac{N_b\Omega^2(\xi^2-1)\widehat{I_a}}{Wh}\right)^{-1}$ terms in Eq's. (23) and (24) thanks to which the trim code could work stable and converge. M_{XX} and M_{YY} are defined in (Ref. 7) as following:

$$M_{XX}=N_b\frac{2}{N_{az}}\sum_{m=1}^{N_{bem}}\left\{\left(\sum_{n=1}^{n=N_{az}}L'_{m,n}\sin\psi_n\right)\left(r_m-\frac{\widehat{I_a}}{\widehat{I_b}}\eta_m\right)\Delta r\right\} \tag{29}$$

$$M_{YY}=N_b\frac{2}{N_{az}}\sum_{m=1}^{N_{bem}}\left\{\left(\sum_{n=1}^{n=N_{az}}L'_{m,n}\cos\psi_n\right)\left(\frac{\widehat{I_a}}{\widehat{I_b}}\eta_m-r_m\right)\Delta r\right\} \tag{30}$$

In Eq's. (23) and (24), flapping angles of the blade are given for leveled trim flight. If these flapping angles are put into the flapping equations (19), (20) and (21) control inputs could be solved. However, it could be easily observed that all the equations of flapping angles and control inputs are coupled. In addition, rotor inflow and blade elastic twists are coupled with rotor flapping angles and control inputs as well. To be able to obtain all the states, an iterative solution procedure is implemented similar to the trim workflow given in (Ref. 9). In Figure 5, details of the iterative trim procedure are shown. In the first step, forward flight speed of the helicopter is defined and all control inputs except the collective input, blade flapping angles, elastic twist field, fuselage aerodynamic drag force and pitching moment, rotor incidence and rolling angle are assumed to be zero. Then, rotor thrust is assumed to be equal to the weight of the helicopter from which collective input and inflow of the main rotor is found. Since collective input is known, elastic field of the rotor, inflow of the rotor, and rotor forces could be found. If the difference between calculated inflow and found inflow in the previous iteration is not in the tolerance limit inflow iteration starts until convergence. After the inflow is converged, elastic twist field iteration starts. If the inflow and elastic twist field are converged, control inputs, blade flapping angles, rotor incidence and rolling angle, fuselage aerodynamic drag force and pitching moments are calculated. If the difference of control inputs and blade flapping angles of two consecutive iteration steps is in the tolerance, trim iterations stop.

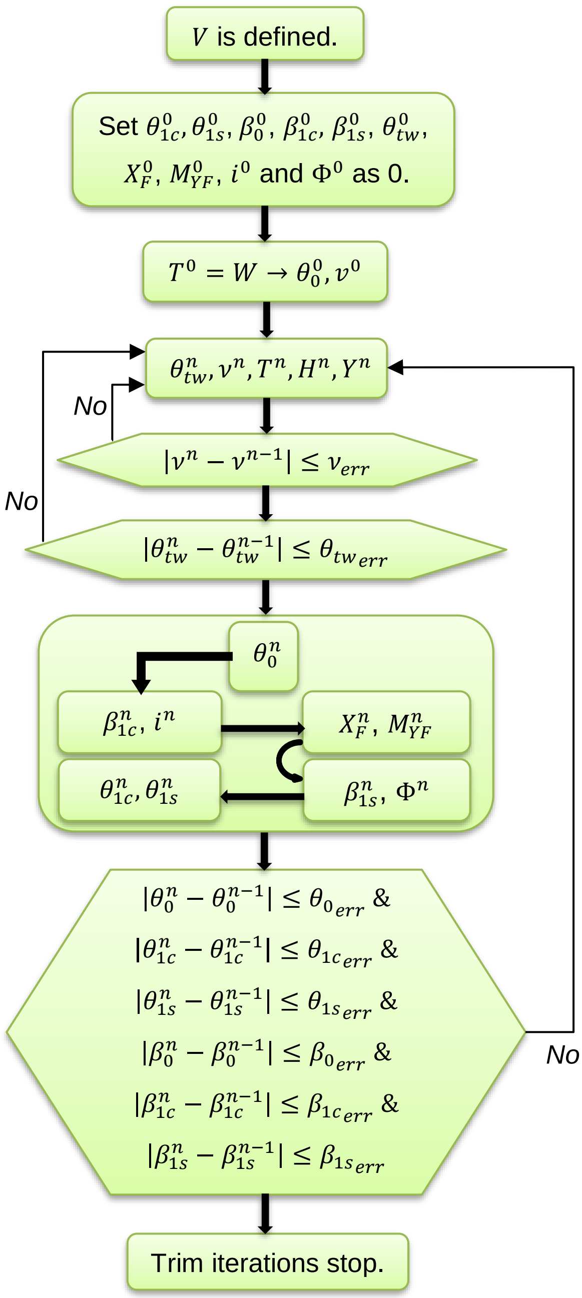

Figure 5: Trim Procedure Workflow.

9. RESULTS

In Figure 6, elastic tip twist of the blade is given. According to the figure, twist is in the order of negative 0.06 degrees. Since aerodynamic center is closer to the trailing edge than the shear center, aerodynamic lift force produced creates a negative pitching moment which twists the blade in the negative direction. Therefore, tip twist of the blade is obtained as negative in Figure 6.

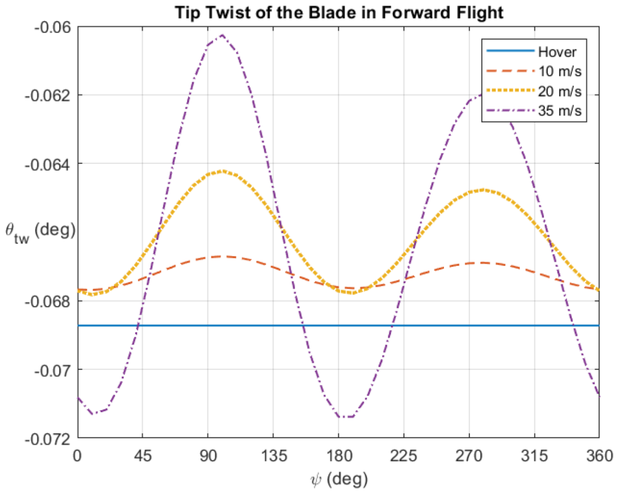

Figure 6: Tip Twist of the Reference Blade for Different Flight Speeds.

Another important observation regarding the tip twist figure is that as the forward flight speed increases, tip twist at the advancing side i.e., $\psi = 90^{o}$ is different than the retreating side's tip twist i.e., $\psi = 180^{o}$. Main reasons behind this situation are the difference of the dynamic pressure between advancing and retreating side, and longitudinal cyclic input θ_{1s} and lateral blade flapping β_{1c}. In hover flight, there is no state changing with azimuth; therefore, in hover blade twist is uniform. However, as the forward flight speed increases, azimuth varying states such as effect of the forward flight speed of the helicopter over the dynamic pressure experienced by the blade, cyclic inputs and flapping angles becomes significant which creates a non-symmetrical distribution of aerodynamic lift force causing a non-symmetrical distribution of the elastic tip twist.

Before making any comment about the magnitude of the torsional deformation of the blade, magnitude of the necessary collective input in a trimmed level flight should be inspected. If Figure 7 is inspected, it is seen that necessary collective input is in the order of 4 to 6 degrees. When the collective input magnitude is compared to the magnitude of the tip twist of the blade, it is found that twist of the blade is much less than the collective input which makes that the difference between rigid blade and elastic blade is small. However, negative tip twist effect is observed in Figure 7. It is observed that necessary collective input in the elastic blade analyses are higher than the rigid blade analyses due to the negative torsional deformation of the blade.

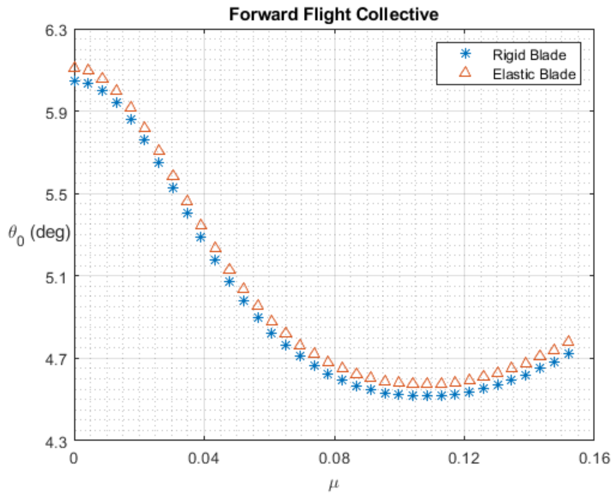

Figure 7: Necessary Collective Input Comparison for Rigid and Elastic Blades in Forward Flight.

In Figure 7, it is also observed that necessary collective input decreases up to some forward flight speed which is one of the main characteristics of the helicopter forward flight analyses. As forward flight speed increases inflow over the main rotor decreases up to some forward flight speed. Therefore, negative effect of the inflow over the angle of attack decrease as well. In other words, as the inflow decreases rotor produces more thrust for a given collective input. As a result, collective input should be decreased up to some forward flight speed to produce same thrust.

Figure 8 shows the nominal required power of the helicopter forward flight. Similar to the collective input decreasing characteristic, required power decreases up to some point as well. In fact, the main reason behind this decrease is same as the collective input. Required power consists of three terms: profile power to rotate the blades in the air, parasite power to move the helicopter in the air, induced power to keep the helicopter in the air. Induced power is directly related to thrust and inflow. Since the inflow decreases with forward flight speed up to some point required power decreases drastically.

However, after some point parasite and profile power dominates the overall required power; as a result, required power graph starts to increase.

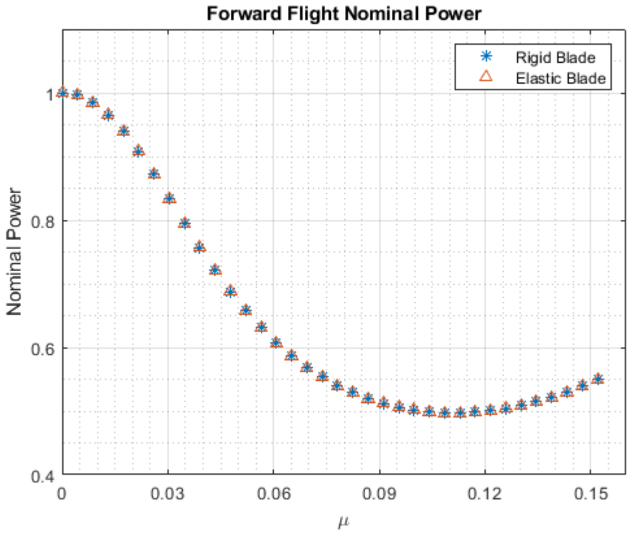

Figure 8: Required Power Comparison for Rigid and Elastic Blades in Forward Flight.

Another important observation regarding Figure 8 is that required power of the elastic blade analysis is almost identical to the required power of the rigid blade analysis. Since parasite power is related to the aerodynamic drag force of the fuselage and forward flight speed of the helicopter and induced power is related to the thrust and inflow, they are almost identical for rigid and elastic blade analyses. Torsional deformation of the elastic blade is very small compared to the collective input. Profile power of rigid and elastic blade are almost identical as well which makes required power of the elastic and rigid blade almost identical.

10. CONCLUSIONS

In this work, torsional deformations of an unmanned helicopter's main rotor blade and their effects to the main rotor collective input and required power of the forward flight speeds are inspected by including compressibility effects. It is observed that although required collective input of the elastic blade analysis is a little higher than the rigid blade, elastic deformations of the blade has little effect on the main rotor collective input and almost no effect on the performance characteristics due to the small magnitude of deformations. Therefore, it could be concluded that the blade might be assumed as rigid in torsional direction for reference helicopter and blade.

Author contact:

Alaaddin Furkan Uzunkaya
alaaddin.uzunkaya@gmail.com

Prof. Dr. Yavuz Yaman yyaman@metu.edu.tr

11. REFERENCES

1. Leishman, J. G., *Principles of Helicopter Aerodynamics*, Cambridge University Press, New York, NY, 2000, Chapter 3.

2. Johnson, W., *Helicopter Theory*, Princeton University Press, Princeton, NJ, 1980, Chapter 2-5.

3. Johnson, W. (2013). *Rotorcraft Aeromechanics*. Cambridge University Press, Chapter 3-5, 15-16

4. Airfoil Tools. (n.d.). NACA 0012 airfoils (n0012-IL). Retrieved October 5, 2022, from http://airfoiltools.com/airfoil/details?airfoil=n0012-il

5. Padfield, G.D. (2007) *Helicopter Flight Dynamics: The Theory and Application of Flying Qualities and Simulation Modelling*. 2nd edn. Oxford: Blackwell. Chapter 3.

6. Anderson, J. D. (2001, January 1). *Fundamentals of Aerodynamics*. McGraw-Hill Science, Engineering & Mathematics. https://doi.org/10.1604/9780072373356 pp. 597-602

7. Uzunkaya, A.F. (2023) *Aeroelastic Analyses of an Unmanned Helicopter*. [MSc. Thesis]. METU. Chapter 4.

8. G. Megson, T. H. (2007). *Aircraft Structures for Engineering Students*. pp. 65-75.

9. Hassan, H., Bayoumy, A., El-Bayoumi, G., & Abdelrahman, M. (2017). Modeling, Trimming and Simulation of a Full Scale Helicopter. *International Conference on Aerospace Sciences and Aviation Technology*, *17,* 1-14. https://doi.org/10.21608/asat.2017.22367

10. Phillips, F. R., White, T. D., Davis, A., & Hartl, D. J. (2022). Analysis of Rotor Blade Aeroelastic Deformation Utilizing the Uncoupled Static Aeroelastic Analysis Method. *AIAA SCITECH 2022 Forum*. https://doi.org/10.2514/6.2022-2555